Peer-reviewed version available at Sensors 2017, 17, 2926; doi:10.3390/s17122926

Article

The impact of the choice of magnetometers and gradiometers in source reconstruction after signal space separation

Pilar Garcés[1,2*], David López-Sanz[1,2,3], Fernando Maestú[1,2,3], and Ernesto Pereda[4]

[1] Laboratory of Cognitive and Computational Neuroscience (UCM-UPM), Centre for Biomedical Technology, Madrid, Spain. E-mails: david.lopez@ctb.upm.es, fernando.maestu@ctb.upm.es
[2] Biomedical Research Networking Center in Bioengineering Biomaterials and Nanomedicine (CIBER-BBN)
[3] Department of Basic Psychology II, Faculty of Psychology, Universidad Complutense de Madrid, Spain
[4] Department of Industrial Engineering, Instituto Universitario de Neurociencia, Universidad de La Laguna, La Laguna, Tenerife, Spain. E-mail: eperdepa@ull.edu.es
* Correspondence: pilar.garceslop@gmail.com; Tel.: (+34) 91 3364642

Abstract: Background: Modern MEG devices include 102 sensor triplets containing one magnetometer and two planar gradiometers. The first processing step is often a signal space separation (SSS), which provides a powerful noise reduction. A question commonly raised by researchers and reviewers is which data should be employed in source reconstruction: (1) magnetometers only, (2) gradiometers only, (3) magnetometers and gradiometers together. The MEG community is currently divided about the proper answer and strong arguments in favor and against these three approaches often expressed. Methods: First, we provide theoretical evidence that both gradiometers and magnetometers contain the same information after SSS, and argue that they both result from the backprojection of the same SSS components. Then, we compare beamforming source reconstructions from magnetometers and gradiometers in real MEG recordings before and after SSS. Results: Without SSS, the correlation between source time series extracted from magnetometers and gradiometers was high, with Pearson correlation coefficient r=0.5-0.8. After SSS, these correlation values increased dramatically, reaching over 0.90 across all cortical areas. Conclusions: After SSS, almost identical source reconstructions (r>0.9) can be obtained with magnetometers and gradiometers, as long as regularization is selected appropriately to account for the different properties in magnetometers and gradiometers covariance matrices.

Keywords: magnetoencephalography; signal space separation; magnetometer; gradiometer; beamforming; regularization

1. Introduction

The signal space separation method (SSS) [1], and its spatiotemporal extension (tSSS) [2] are powerful noise reduction methods commonly used as a first preprocessing step in raw MEG data. In fact, they have repeatedly been proven to be successful in the suppression of unwanted magnetic noise originating from distant [3] to nearby [2] sources, or even from orthodontic material [4]. Also, the use of device-independent coordinates in SSS enables to compensate for head movements inside the MEG scanner [2]. Roughly, this is achieved by considering the raw MEG data as a superposition of harmonic components, which originate either inside or outside the brain (or rather, a sphere that is fitted individually and lies inside the MEG helmet). SSS discards the external components and produces a cleaner version of the MEG data by backprojecting the internal components exclusively.

The use of SSS is particularly widespread in modern Elekta Neuromag® (Vectorview and TRIUX) MEG systems, and it can be easily applied directly at the workstations with Maxfilter™ [5] or with MNE software (from version 0.11 onwards [6]). These new systems are equipped with 306

sensors, grouped into 102 elements with one magnetometer and two orthogonal planar gradiometers each [7]. Magnetometers measure the normal component of the magnetic field at the sensor's position $B_z(\vec{r})$ and are sensible to fields originating within a wide distance. Planar gradiometers, instead, estimate the spatial derivative of $B_z(\vec{r})$ in two orthogonal directions perpendicular to the MEG helmet (i.e. $\frac{\partial B_z(\vec{r})}{\partial x}$ and $\frac{\partial B_z(\vec{r})}{\partial y}$) , so that their sensitivity decreases faster with distance, hence, they are less sensitive to distant sources and more robust to environmental interference [8,9]. Both magnetometers and gradiometers measure tiny magnetic fields, typically in the range of 10^{-11}-10^{-9} T and 10^{-11}-$5{\cdot}10^{-10}$ T/m respectively.

Although the availability of these two sensor types at each location is very appealing, it also creates some controversy on the appropriate analysis pipeline. This is particularly the case when performing source reconstruction. Researchers in the field follow typically three different approaches for this purpose: (1) using gradiometers only (2) using magnetometers only, or (3) using both sensor types, after applying some scaling factor that yields a similar variance in the time series of both data types. All of these options have strong supporters and critics amongst experimenters and reviewers, and arguments such as: "magnetometers can detect deeper sources," "gradiometers are less noisy," or "using magnetometers only (gradiometers only) means discarding 2/3 (1/3) of the data" are often heard. However, are these arguments valid after SSS?

In this work, we address this question and argue that, after (t)SSS, magnetometers and gradiometers contain the same information. That is, gradiometers and magnetometers yield source reconstructions that are essentially equivalent, as long as the properties of both sensor types are taken into account, in the case of beamforming, by choosing appropriate regularization factors. To tackle this issue, we provide a theoretical argumentation and compare experimentally the source reconstructions estimated from magnetometers and gradiometers, with and without SSS.

2. Materials and Methods

2.1 Theoretical reasoning

The initial assumption in SSS is the presence of three separate volumes: (a) an inner volume containing the inside (brain) currents $\boldsymbol{j}_{in}$, (b) an intermediate volume which includes the MEG sensors and is current-free and (c) an outer volume containing the external currents $\boldsymbol{j}_{out}$. The magnetic field $\boldsymbol{B}(\boldsymbol{r})$ at a source-free sensor position, $\boldsymbol{r}$ is the superposition of the fields created by $\boldsymbol{j}_{in}$ and $\boldsymbol{j}_{out}$:

$$\boldsymbol{B}(\boldsymbol{r}) = \boldsymbol{B}_{in}(\boldsymbol{r}) + \boldsymbol{B}_{out}(\boldsymbol{r}). \quad (1)$$

As proven in [1,10], under the quasistatic approximation, $\boldsymbol{B}_{in}(\boldsymbol{r})$ and $\boldsymbol{B}_{out}(\boldsymbol{r})$ can be written as separate series expansions:

$$\boldsymbol{B}_{in}(\boldsymbol{r}) = \sum_{l=1}^{\infty}\sum_{m=-l}^{l} \alpha_{lm}\boldsymbol{F}(\boldsymbol{r}), \quad (2)$$

$$\boldsymbol{B}_{out}(\boldsymbol{r}) = \sum_{l=1}^{\infty}\sum_{m=-l}^{l} \beta_{lm}\boldsymbol{G}(\boldsymbol{r}), \quad (3)$$

where $\boldsymbol{F}(\boldsymbol{r})$ and $\boldsymbol{G}(\boldsymbol{r})$ are functions derived from spherical harmonics and scale with $1/r^{l+2}$ and r^l respectively. For the sake of brevity, their analytic formulation is not written here, but can be found elsewhere [1]. α_{lm} and β_{lm} are coefficients that depend on the current distributions $\boldsymbol{j}_{in}$ and $\boldsymbol{j}_{out}$, and are independent of the target position $\mathbf{r}$.

$\boldsymbol{B}_{in}$ and $\boldsymbol{B}_{out}$ at each of the MEG coils position $\boldsymbol{r}_1, \dots, \boldsymbol{r}_{Ncoils}$ can then be expressed as a linear combination of α_{lm} and β_{lm}, after truncating (2) and (3) to $l \le L_{in}$ and $l \le L_{out}$ respectively and computing $\boldsymbol{F}(\boldsymbol{r})$ and $\boldsymbol{G}(\boldsymbol{r})$ at $\boldsymbol{r}_1, \dots, \boldsymbol{r}_{Ncoils}$. The series expansions are usually truncated to $L_{in} = 8$ and $L_{out} = 3$, since they are considered to produce a negligible residual [1,3]. This would yield $n_{in} = (L_{in}+1)^2 - 1 = 80$ inside terms and $n_{out} = (L_{out}+1)^2 - 1 = 15$ outside terms.

Then, the magnetic field (normal component) at the coils' position can be written as:

$$B_{coil} \approx \left[\boldsymbol{T}_{in,coil}\ \boldsymbol{T}_{out,coil}\right]\begin{bmatrix}\boldsymbol{x}_{in}\\ \boldsymbol{x}_{out}\end{bmatrix}, \quad (4)$$

where $\boldsymbol{T}_{in,coil}$ and $\boldsymbol{T}_{out,coil}$ are $N_{coils} \times n_{in}$ and $N_{coils} \times n_{out}$ matrices respectively, which are computed from the system's geometry based on $\boldsymbol{F}(\boldsymbol{r})$ and $\boldsymbol{G}(\boldsymbol{r})$; and $\boldsymbol{x}_{in}$ and $\boldsymbol{x}_{out}$ are vectors of length n_{in} and n_{out} that contain the α_{lm} and β_{lm} coefficients.

If one takes into account that $M_i = B_{coil,j}$ for magnetometers and $M_i = B_{coil,j} - B_{coil,k}$ for gradiometers, the MEG measurements **M** can be similarly expressed as a matrix product:

$$\boldsymbol{M} \approx \boldsymbol{S}\boldsymbol{x} = \left[\boldsymbol{S}_{in}\ \boldsymbol{S}_{out}\right]\begin{bmatrix}\boldsymbol{x}_{in}\\ \boldsymbol{x}_{out}\end{bmatrix}, \quad (5)$$

where the rows of $\boldsymbol{S}_{in}$ ($\boldsymbol{S}_{out}$) are rows of $\boldsymbol{T}_{in,coil}$ ($\boldsymbol{T}_{out,coil}$) for magnetometers and are the subtraction of two $\boldsymbol{T}_{in,coil}$ ($\boldsymbol{T}_{out,coil}$) rows for gradiometers.

Finally, the inside and outside components are estimated from $\hat{\boldsymbol{x}} = \begin{bmatrix}\boldsymbol{x}_{in}\\ \boldsymbol{x}_{out}\end{bmatrix} = \boldsymbol{S}^{-1}\boldsymbol{M}$, and a cleaner version of the MEG measurements is estimated by projecting the inside components only:

$$\widehat{\boldsymbol{M}_{in}} \approx \boldsymbol{S}_{\boldsymbol{in}}\hat{\boldsymbol{x}}_{\boldsymbol{in}}. \quad (6)$$

In summary, the inside components $\boldsymbol{x}_{in}$ are estimated using all channels, magnetometers or gradiometers (bad channels should of course be discarded), and, after SSS, the activity of both sensor types derives from the projection of the same n_{in} components.

2.2. Experimental source reconstructions from magnetometers and gradiometers

To further explore the relation between magnetometers and gradiometers after SSS, in this section we compare source reconstructions estimated separately from both sensor types in real MEG recordings

2.2.1. MEG acquisition and source estimation

The resting state data used here was recorded for a test-retest reliability project. Details on data acquisition, preprocessing, and source reconstruction can be found in [11]. Briefly, 4 min resting state eyes closed data from 16 healthy subjects (age 30.4 ± 5.8, ten female) were employed here. MEG recordings were acquired with an Elekta Vectorview system with 306 sensors (102 magnetometers and 204 planar gradiometers), inside a magnetically shielded room (Vacuumschmelze GmbH, Hanau, Germany). Subjects' heads were digitized with a Fastrak Polhemus, and four coils were attached to the forehead and mastoids so that the head position on the MEG helmet was continuously determined. Activity in electrooculogram channels was also recorded to keep track of ocular artifacts. Signals were sampled at 1000 Hz with an online filter of bandwidth 0.1-300 Hz.

SSS and tSSS were applied to the raw resting state data with Maxfilter (version 2.2) and its default parameters (L_{in}=8, L_{out}=3, tSSS correlation window=10s, and tSSS correlation limit=0.9). We note that although the data presented in subsequent sections corresponds to the SSS-filtered dataset, we obtained similar results with tSSS. Bad channels were visually detected and not included in the SSS/tSSS estimation. Jump, muscle and ocular artefacts were detected using FieldTrip [12], and non-overlapping artefact-free 6-second epochs were located. Data was bandpass filtered in [2-30]Hz with a finite impulse response (FIR) filter of order 1000.

Source and forward models were built individually after segmenting each subject's T1-weighted MRI with Freesurfer (version 5.1.0), [13,14], downsampling and realigning surfaces, and estimating leadfield matrices with MNE software [6]. Linearly constrained minimum variance (LCMV) beamformer [15] was used to perform source reconstruction. For each subject and source, we computed beamformer filters as:

$$\boldsymbol{w}_{\boldsymbol{i}} = \left[\boldsymbol{L}_{\boldsymbol{i}}^{\boldsymbol{T}}\boldsymbol{C}_{\boldsymbol{inv}}\boldsymbol{L}_{\boldsymbol{i}}\right]^{-\mathbf{1}}\boldsymbol{L}_{\boldsymbol{i}}^{\boldsymbol{T}}\boldsymbol{C}_{\boldsymbol{inv}}, \quad (7)$$

where $\boldsymbol{L}_{\boldsymbol{i}}$ is the $N_{sensors} \times 3$ leadfield matrix for source i, and $\boldsymbol{C}_{\boldsymbol{inv}}$ is a $N_{sensors} \times N_{sensors}$ estimate of the inverse of the sensor's covariance matrix $\boldsymbol{C}$:

$$\boldsymbol{C}_{\boldsymbol{inv}} = pinv\left(\boldsymbol{C} + \lambda\frac{trace(\boldsymbol{C})}{N_{sensors}}\boldsymbol{I}\right), \quad (8)$$

Preprints (www.preprints.org) | NOT PEER-REVIEWED | Posted: 27 October 2017 doi:10.20944/preprints201710.0165.v1

Peer-reviewed version available at Sensors 2017, 17, 2926; doi:10.3390/s17122926

where $\boldsymbol{I}$ is the identity matrix and λ>0 is called the regularization factor. Regularizing is equivalent to adding uncorrelated noise to the sensor measurements, and it is necessary for the stability of the inversion of the covariance matrix $\boldsymbol{C}$. This is especially crucial after SSS, since it projects back only 60-80 inside coefficients, and yields rank-deficient covariance matrices. In this work, we have defined the regularization parameter λ as the average diagonal of the covariance matrix, which is a common convention in the literature [16], and it is used in the popular FieldTrip toolbox [12]. The robustness of the $\boldsymbol{C_{inv}}$ matrix inversion can be quantified through:

$$cn = \mathrm{cond}\left(\boldsymbol{C} + \lambda \frac{trace(\boldsymbol{C})}{N_{sensors}} \boldsymbol{I}\right), \quad (9)$$

where *cond* refers to the 1-norm condition number.

For each source location $\boldsymbol{i}$, the orientation $\boldsymbol{\eta_i}$ was determined as the one maximizing the source power $\boldsymbol{w_i}^T \boldsymbol{C} \boldsymbol{w_i}$, and the beamforming filter was projected into this direction: $\boldsymbol{w_{i,\eta}} = \boldsymbol{\eta_i} \boldsymbol{w_i}$. Finally, we derived source time series as:

$$\boldsymbol{s_i(t)} = \boldsymbol{w_{i,\eta}} \boldsymbol{M(t)}. \quad (10)$$

For each subject, source time series were extracted for magnetometers and gradiometers separately for varying regularization parameters λ_{mag} and λ_{grad}. The similarity between magnetometer and gradiometer source reconstructions was evaluated with the Pearson correlation between reconstructed source time series. The effect of the magnetometers vs. gradiometer choice on resting state powerspectrum and functional connectivity estimates was evaluated with intraclass correlation coefficient (ICC type 1-1, following [17]).

3. Results

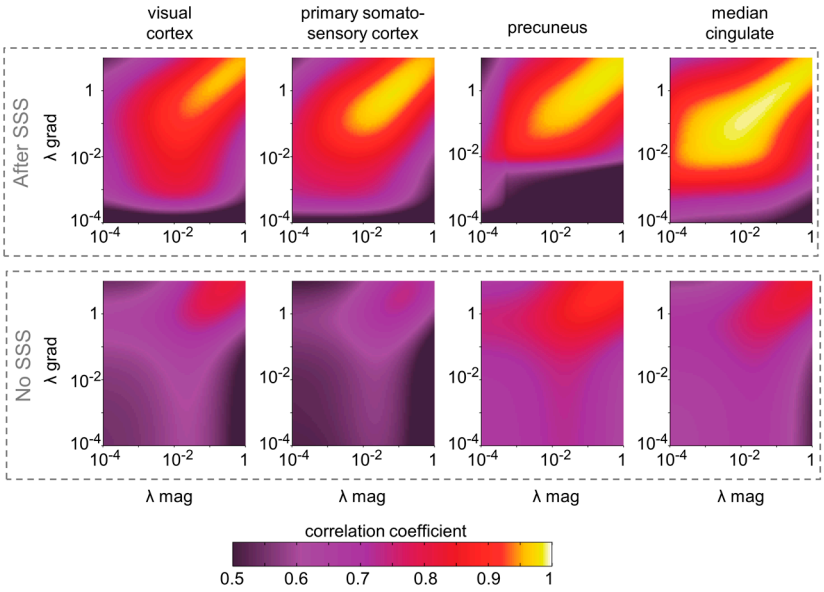

Figure 1. Correlation between source time series derived from magnetometers and gradiometers with and without SSS. Pearson correlation coefficients averaged across subjects are shown for five selected sources as a function of the regularization parameters λ for magnetometer (x-axis) and gradiometer (y-axis) beamforming reconstructions. The selected sources were located in MNI space: visual cortex (MNI: -41, -77, 3), primary somatosensory cortex (MNI: -38 -27 52), precuneus (MNI: 1 -57 28) and median cingulate (MNI: -2 12 40).

3.1. Correlation between magnetometer and gradiometer source reconstructions after SSS, as a function of the regularization factor λ

For each subject, we computed source reconstruction separately for magnetometers and gradiometers, with and without SSS for 80 regularization factors between $\lambda = 10^{-4}$ and $\lambda = 1$. We chose for this analysis four representative sources located in exemplary cortical areas: visual cortex (MNI

Preprints (www.preprints.org) | NOT PEER-REVIEWED | Posted: 27 October 2017 doi:10.20944/preprints201710.0165.v1

Peer-reviewed version available at Sensors 2017, 17, 2926; doi:10.3390/s17122926

coordinates [-41 -77 3]mm), primary somatosensory cortex (MNI: [-38, -27, 52]mm), precuneus (MNI: [1, -57, 28]mm) and median cingulate (MNI: [-2, 12, 40]mm). The Pearson correlation coefficients r were computed between source time series derived from magnetometers and gradiometers for each pair of λ_{mag} and λ_{grad} and averaged over trials and subjects (see Figure 1). Without SSS, correlation coefficients were moderate, ranging between 0.4 and 0.8, and reaching their highest values (0.8-0.9) for high regularizations approaching λ=1. However, they were much higher for SSS-filtered data, reaching values of r> 0.9 for λ_{mag} and λ_{grad} >0.01. The λ_{mag} and λ_{grad} reaching the highest values of r>0.95 were positively related, in a seemingly log-log dependence. Of note, equivalent results were obtained when comparing the source reconstructions using each type of sensor separately with that obtained with the whole magnetometer + gradiometer dataset, normalizing the variance of both sensor types as in [18]. Results can be found in Supplementary Figure 1.

We further explored this dependence by selecting, for each source and λ_{mag} separately, the λ_{grad} for which the highest *r* was obtained. As shown in Figure 2, the relation between $\lambda_{mag,max}$ and $\lambda_{grad,max}$ was indeed monotonically increasing in a rather linear fashion for λ_{mag} > 0.01. The least squares fit that best reproduced this relation was: $\log_{10}(\lambda_{grad,max})$ = 0.574*$\log_{10}(\lambda_{mag,max})$ + 0.611 (r^2 = 0.96). This means that a higher regularization is necessary for gradiometers than for magnetometers to obtain an equivalent source reconstruction. For instance, for a λ_{mag}=0.01, the corresponding λ_{grad} yielding the most similar source reconstructions is λ_{grad}=0.29. When focusing on the condition numbers of $\boldsymbol{C} + \lambda \frac{trace(\boldsymbol{C})}{N_{sensors}} \boldsymbol{I}$ instead of the regularization factors λ, we also observed a rather linear and positive relation between $cn_{mag,max}$ and $cn_{grad,max}$ (minimum-square linear fit: $\log_{10}(cn_{grad,max})$ = 0.590*$\log_{10}(cn_{mag,max})$ + 0.886, r^2 = 0.96). Lower covariance matrix condition numbers (or more invertible matrices) are needed for gradiometers than for magnetometers to produce equivalent source reconstructions.

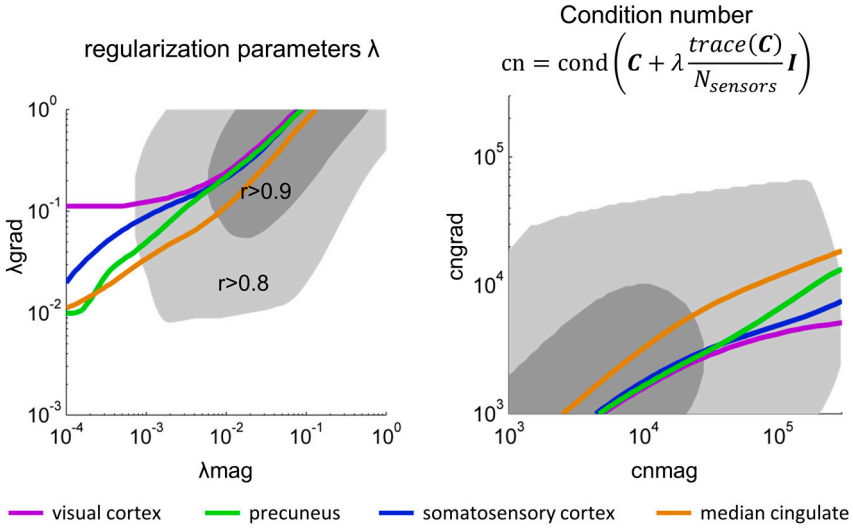

Figure 2. The correlation between magnetometer and gradiometer source reconstruction after SSS depends on the regularization parameter λ and the condition number cn of the sensor covariance matrix. In the left, the lines display, for each λ_{mag}, the λ_{grad} that yields maximum subject average correlation r between magnetometer and gradiometer source reconstructions. The gray surfaces span the area for which r>0.8 (lighter gray) and r>0.9 (darker gray) for all five sources considered. In the right side, an equivalent plot is built with axes corresponding to the condition numbers of the regularized magnetometers and gradiometers covariance matrices (cnmag and cngrad respectively).

3.2. Spatial dependence of the correlation between magnetometer and gradiometer source reconstructions

To evaluate the whole-brain spatial relationship between magnetometer and gradiometer source reconstructions, we separately computed the correlations between source time series extracted with both sensor types using λ_{mag}=0.01 and λ_{grad}=0.29 respectively for all cortical sources.

Peer-reviewed version available at Sensors 2017, 17, 2926; doi:10.3390/s17122926

Figure 3 shows the spatial distribution of the average correlation coefficient r between magnetometer and gradiometers source reconstructions across subjects, using both the raw and the SSS-filtered datasets. After SSS, r>0.9 was found for all sources, indicating an almost identical source estimation for both sensor types. This correlation was much weaker for the raw dataset without SSS, with r = 0.4-0.7 for most cortical regions and r>0.7-0.85 for posterior and deeper regions around visual cortex, posterior cingulate and precuneus. When comparing source reconstructions with and without SSS, the former were more strongly correlated (r>0.7) with raw magnetometer source reconstructions in posterior central, parietal, and posterior regions and with raw gradiometer source reconstructions in frontal, temporal and cingulate regions.

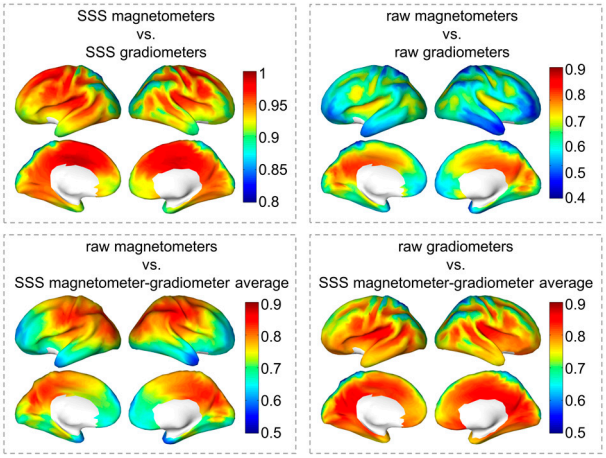

Figure 3. Correlation between source time series for λ_{mag} = 0.01 and λ_{grad} = 0.29. The brain surfaces display the subject-averaged Pearson correlation coefficients between pairs of source time series estimated with different sensor types and with/without SSS. Note that the limits of the color bars differ across panels.

3.3. Inter-pipeline reliability of power and functional connectivity values: impact on the choice of magnetometers or gradiometers.

One may argue that the above results only apply to the reconstructed source time series in the time domain, whereas the spectral properties or the functional connectivity (FC) patterns obtained from both types of sensors may differ. To estimate the impact that the choice of magnetometers or gradiometers would have in the outcome of the spectral properties and FC in a real experiment, we quantified the difference between magnetometer and gradiometer-derived values of these target measures. Power spectra were calculated from source time series with the multitaper method using Hamming windows and 1Hz smoothing and normalized to the overall power in the [2-30]Hz. We estimated relative power for the following frequency bands: delta ([2-4]Hz), theta ([4-8]Hz), alpha ([8-13]Hz) and beta ([13-30]Hz), and averaged over the 66 cortical regions of the Desikan-Killiany atlas [19]. As an estimate of FC, we computed the phase locking value (PLV) between all pairs of regions in the delta, theta, alpha, and beta bands. More details on the implementation of power and PLV estimation can be found in [11,20].

The inter-analysis pipeline reliability of the power and PLV estimates was quantified with the intraclass correlation coefficient (ICC type 1-1, following [17]), comparing power and PLV values obtained with magnetometers and regularization λ=0.01 and gradiometers with regularization λ=0.29. Figure 4 shows the distribution of ICC values across regions and links. For comparison, we also computed the reliability between the analysis pipelines using magnetometers only but different λ coefficients (always keeping the option magnetometers with λ=0.01 as a reference) and included in Figure 4. We found excellent inter-pipeline reliability (ICC>0.85) for the power spectra for all analysis pipeline combinations. ICC values for PLV were however smaller. Although for more than 3/4 of the links ICC>0.8, which is usually regarded as an excellent reliability [21], the ICC values spanned a broader interval ([0.4-1]) when comparing mag-λ=0.01 and grad-λ=0.29. This was

however also the case when comparing mag-λ=0.01 and mag-λ=0.05. To further evaluate whether the impact on reliability was driven by the regularization or by the sensor choice, the dependence between ICC values obtained with grad-λ=0.29 and mag-λ=0.05 (keeping mag-λ=0.01 as a reference) was explored (Figure 4-C). Both magnitudes were strongly correlated (Pearson r=0.36-0.51, p-value<10^{-10}). This means that the links with smaller ICC in grad-λ=0.29 tend to be also the links with smaller Icc in mag-λ=0.05. This fact indicates it is the regularization intensity rather than the sensor choice which causes the drop on ICC.

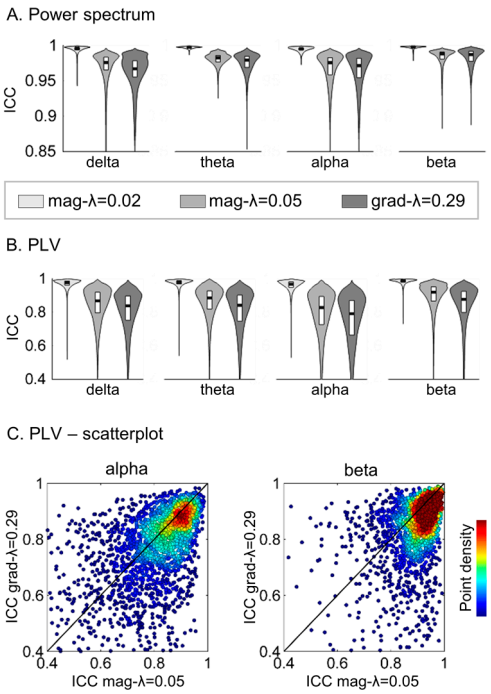

Figure 4. Inter-pipeline reliability of power spectrum and phase locking value (PLV) estimates. The reliability was evaluated with the ICC (Intraclass correlation coefficient), using as a reference the mag-λ=0.01 pipeline (choosing magnetometers for source reconstruction and a regularization factor of λ=0.01). We compared three pipelines against this reference: mag-λ=0.02 (using magnetometers and λ=0.02), mag-λ=0.05 (using magnetometers and λ=0.05) and grad-λ=0.29 (using gradiometers and λ=0.29). A. Violin plots of the distribution of Icc coefficients for relative power estimates in the delta, alpha, beta and gamma bands across the 66 cortical regions of the Desikan-Killiany atlas. B. Violin plots of the distribution of ICC for PLV across pairs of regions (or links) for each frequency band. C. Scatterplot of the ICC values obtained with the mag-λ=0.05 and the grad-λ=0.29 pipelines. Each dot represents a single connection, and the color displays the density of points.

4. Discussion

In this work, we have demonstrated both theoretically and experimentally that magnetometer and gradiometer data after SSS contain equivalent information, and therefore produce very similar source reconstructions (Pearson correlation coefficient > 0.9). Although these results may not come as a surprise for most Elekta users experienced with SSS and source reconstruction, there is substantial controversy in the general neuroimaging community on the selection of magnetometers and gradiometers. The present work provides a focused analysis on this issue, which we hope will guide MEG users who are designing analysis plans, contribute to avoiding additional lengthy discussions during scientific peer-review, and inform researchers who are doubtful about the different source reconstruction approaches.

Currently, the source reconstruction literature using Elekta MEG devices is divided among different options: using magnetometers only [22], gradiometers only [23], both sensor types simultaneously [24,25], or both sensor types separately across main manuscript and supplementary information: [20]. In this work, we have demonstrated that all these approaches are equivalent,

given that all the cited works used SSS for MEG data denoising. We note however that the choice of magnetometers and gradiometers is relevant when working in sensor space since both sensor types yield different topographies for the same source activation. While magnetometers have a circular sensitivity distribution, planar gradiometers have maximum sensitivity directly under the sensors [8]. Furthermore, planar gradiometers can be combined to produce sensor-space pseudo current maps, which provide a more accurate estimation of the underlying current distribution than magnetometer-derived topographies[26].

A crucial factor to ensure comparability between magnetometer and gradiometer source reconstructions is an appropriate regularization of the covariance matrices. The importance of regularization in MEG/EEG beamforming has been established previously [27–29]. Brookes et al. [30] demonstrated that shorter experiment times, smaller frequency bandwidths and increasing amount of sensors produce a higher error in the covariance matrix estimation and therefore require greater regularization, which comes at the expense of a loss in spatial resolution. After (t)SSS, the effective dimensionality of magnetometer and gradiometer covariance matrices is equal to the number of inside SSS components, which is typically in the range 60-80. Since Elekta MEG devices contain twice as many gradiometers than magnetometers, after SSS the gradiometer covariance matrix has a higher condition number (is less invertible) than the magnetometer covariance matrix. A greater regularization is, therefore, necessary for gradiometers than for magnetometers. In particular, we found that the relation between the regularization coefficients producing most strongly correlated source reconstructions for both sensor types is: $\log_{10}(\lambda_{grad,max}) = 0.574*\log_{10}(\lambda_{mag,max}) + 0.611$.

Although selecting higher regularizations for gradiometers than for magnetometers yields comparable condition numbers and most highly correlated source time series, having different regularization intensities (and therefore the different intensity of added noise) can affect the spatial properties of magnetometers and gradiometers. To explore this, we evaluated the inter-pipeline reliability of conventional MEG measures (power and functional connectivity) obtained with magnetometers with λ=0.01 and gradiometers with λ=0.29 (combination yielding source time series correlation > 0.9). Power values estimated with both analysis pipelines were remarkably similar (ICC>0.85). Functional connectivity values were more variable: although for most links and frequency bands ICC>0.8, ICC values in the [0.4-0.8] range were also obtained. ICC comparing pipelines using magnetometers only and different λ were similarly affected, indicating that the regularization is causing the difference in FC estimates obtained with magnetometers and gradiometers. Such result is not particularly surprising since the effect of regularization on the spatial resolution of source reconstruction is well-known [27–29].

5. Conclusions

We have demonstrated that magnetometer and gradiometer data after SSS contain the same information (originating from the same SSS inside components) and can generate equivalent beamforming source reconstructions, as long as appropriate regularization strengths are chosen for both sensor types. We have provided a theoretical reasoning and an experimental framework for this argument. Source time series estimated with both sensor types after SSS are correlated over 0.9, and the average inter-pipeline reliability of power and functional connectivity was strong to excellent (with average ICCs of 0.8-0.98). This result unifies different analysis pipelines existing in the literature and proves that, while the choice of magnetometers or gradiometers in source reconstruction after SSS has a minimal impact on the outcomes of MEG studies and, the selection of the regularization strength has a stronger effect on functional connectivity estimates.

Supplementary Materials: Comparison of single sensor type reconstructed source time series with source time series reconstructed with the whole (magnetometer+gradiometer) dataset can be found online at www.mdpi.com/link, Figure S1 Correlation between source time series derived from magnetometers only and (magnetometers+gradiometers) depending on the λ regularization parameter.

Acknowledgments: This work was supported by project TEC2016-80063-C3-2-R from the Spanish MINECO. We thank María Carmen Martín-Buro for her work in MEG data acquisition and Ricardo Bruña for his valuable comments on the manuscript.

Author Contributions: P.G, E.P., F.M. conceived, designed and performed the experiments; P.G and D.L. analyzed the data; P.G. and E.P drafted the first manuscript, all the authors revised and agreed on the final version of the manuscript.

Conflicts of Interest: The authors declare no conflict of interest.

References

1. Taulu, S.; Kajola, M. Presentation of electromagnetic multichannel data: The signal space separation method. *J. Appl. Phys.* **2005**, *97*, 124905, doi:10.1063/1.1935742.
2. Taulu, S.; Simola, J. Spatiotemporal signal space separation method for rejecting nearby interference in MEG measurements. *Phys. Med. Biol.* **2006**, *51*, 1759–68, doi:10.1088/0031-9155/51/7/008.
3. Taulu, S.; Simola, J.; Kajola, M. Applications of the signal space separation method. *IEEE Trans. Signal Process.* **2005**, *53*, 3359–3372, doi:10.1109/TSP.2005.853302.
4. Hillebrand, A.; Fazio, P.; de Munck, J. C.; van Dijk, B. W. Feasibility of clinical Magnetoencephalography (MEG) functional mapping in the presence of dental artefacts. *Clin. Neurophysiol.* **2013**, *124*, 107–113, doi:10.1016/j.clinph.2012.06.013.
5. Elekta-Neuroscience MaxFilter User's Guide. Software version 2.2 2010.
6. Gramfort, A.; Luessi, M.; Larson, E.; Engemann, D. A.; Strohmeier, D.; Brodbeck, C.; Parkkonen, L.; Hämäläinen, M. S. MNE software for processing MEG and EEG data. *Neuroimage* **2014**, *86*, 446–60, doi:10.1016/j.neuroimage.2013.10.027.
7. Elekta-Neuromag *Elekta Neuromag® System Hardware User Manual*; 2005;
8. Malmivuo, J.; Plonsey, R. Magnetoencephalography. In *Bioelectromagnetism: principles and applications of bioelectric and biomagnetic fields*; Oxford University Press: New York Oxford, 1995.
9. Vrba, J.; Robinson, S. E. SQUID sensor array configurations for magnetoencephalography applications. *Supercond. Sci. Technol.* **2002**, *15*, R51–R89, doi:10.1088/0953-2048/15/9/201.
10. Gauss, C. F. Allgemeine Theorie des Erdmagnetismus. In *Werke*; Springer Berlin Heidelberg: Berlin, Heidelberg, 1877; pp. 119–193.
11. Garcés, P.; Martín-Buro, M. C.; Maestú, F. Quantifying the Test-Retest Reliability of Magnetoencephalography Resting-State Functional Connectivity. *Brain Connect.* **2016**, *6*, 448–460, doi:10.1089/brain.2015.0416.
12. Oostenveld, R.; Fries, P.; Maris, E.; Schoffelen, J.-M. FieldTrip: Open source software for advanced analysis of MEG, EEG, and invasive electrophysiological data. *Comput. Intell. Neurosci.* **2011**, *2011*, 156869, doi:10.1155/2011/156869.
13. Fischl, B.; Salat, D. H.; Busa, E.; Albert, M.; Dieterich, M.; Haselgrove, C.; van der Kouwe, A.; Killiany, R.; Kennedy, D.; Klaveness, S.; Montillo, A.; Makris, N.; Rosen, B.; Dale, A. M. Whole Brain Segmentation. *Neuron* **2002**, *33*, 341–355, doi:10.1016/S0896-6273(02)00569-X.
14. Ségonne, F.; Pacheco, J.; Fischl, B. Geometrically accurate topology-correction of cortical surfaces using nonseparating loops. *IEEE Trans. Med. Imaging* **2007**, *26*, 518–29, doi:10.1109/TMI.2006.887364.
15. Van Veen, B. D.; van Drongelen, W.; Yuchtman, M.; Suzuki, A. Localization of brain electrical activity via linearly constrained minimum variance spatial filtering. *IEEE Trans. Biomed. Eng.* **1997**, *44*, 867–80, doi:10.1109/10.623056.
16. Litvak, V.; Eusebio, A.; Jha, A.; Oostenveld, R.; Barnes, G. R.; Penny, W. D.; Zrinzo, L.; Hariz, M. I.; Limousin, P.; Friston, K. J.; Brown, P. Optimized beamforming for simultaneous MEG and intracranial

local field potential recordings in deep brain stimulation patients. *Neuroimage* **2010**, *50*, 1578–1588, doi:10.1016/j.neuroimage.2009.12.115.

17. Shrout, P.; Fleiss, J. Intraclass correlations: uses in assessing rater reliability. *Psychol. Bull.* **1979**.
18. Hunt, L. T.; Woolrich, M. W.; Rushworth, M. F. S.; Behrens, T. E. J. Trial-Type Dependent Frames of Reference for Value Comparison. *PLoS Comput. Biol.* **2013**, *9*, e1003225, doi:10.1371/journal.pcbi.1003225.
19. Desikan, R. S.; Ségonne, F.; Fischl, B.; Quinn, B. T.; Dickerson, B. C.; Blacker, D.; Buckner, R. L.; Dale, A. M.; Maguire, R. P.; Hyman, B. T.; Albert, M. S.; Killiany, R. J. An automated labeling system for subdividing the human cerebral cortex on MRI scans into gyral based regions of interest. *Neuroimage* **2006**, *31*, 968–80, doi:10.1016/j.neuroimage.2006.01.021.
20. Martín-Buro, M. C.; Garcés, P.; Maestú, F. Test-retest reliability of resting-state magnetoencephalography power in sensor and source space. *Hum. Brain Mapp.* **2016**, *37*, 179–190, doi:10.1002/hbm.23027.
21. Cicchetti, D. V.; V., D. Guidelines, criteria, and rules of thumb for evaluating normed and standardized assessment instruments in psychology. *Psychol. Assess.* **1994**, *6*, 284–290, doi:10.1037/1040-3590.6.4.284.
22. García-Pacios, J.; Garcés, P.; Del Río, D.; Maestú, F. Early detection and late cognitive control of emotional distraction by the prefrontal cortex. *Sci. Rep.* **2015**, *5*, 10046, doi:10.1038/srep10046.
23. Wens, V.; Bourguignon, M.; Goldman, S.; Marty, B.; Op de Beeck, M.; Clumeck, C.; Mary, A.; Peigneux, P.; Van Bogaert, P.; Brookes, M. J.; De Tiège, X. Inter- and intra-subject variability of neuromagnetic resting state networks. *Brain Topogr.* **2014**, *27*, 620–34, doi:10.1007/s10548-014-0364-8.
24. Hillebrand, A.; Tewarie, P.; van Dellen, E.; Yu, M.; Carbo, E. W. S.; Douw, L.; Gouw, A. A.; van Straaten, E. C. W.; Stam, C. J. Direction of information flow in large-scale resting-state networks is frequency-dependent. *Proc. Natl. Acad. Sci. U. S. A.* **2016**, *113*, 3867–72, doi:10.1073/pnas.1515657113.
25. Henson, R. N.; Mouchlianitis, E.; Friston, K. J. MEG and EEG data fusion: Simultaneous localisation of face-evoked responses. *Neuroimage* **2009**, *47*, 581–589, doi:10.1016/j.neuroimage.2009.04.063.
26. Haberkorn, W.; Steinhoff, U.; Burghoff, M.; Kosch, O.; Morguet, A.; Koch, H. Pseudo current density maps of electrophysiological heart, nerve or brain function and their physical basis. *Biomagn. Res. Technol.* **2006**, *4*, 5, doi:10.1186/1477-044X-4-5.
27. Sekihara, K.; Nagarajan, S. S. *Adaptive Spatial Filters for Electromagnetic Brain Imaging*; Springer, 2008; ISBN 3540793704.
28. Dalal, S. S.; Zumer, J. M.; Guggisberg, A. G.; Trumpis, M.; Wong, D. D. E.; Sekihara, K.; Nagarajan, S. S. MEG/EEG source reconstruction, statistical evaluation, and visualization with NUTMEG. *Comput. Intell. Neurosci.* **2011**, *2011*, 758973, doi:10.1155/2011/758973.
29. Hillebrand, A.; Barnes, G. R. Beamformer Analysis of MEG Data. *Int. Rev. Neurobiol.* **2005**, *68*, 149–171, doi:10.1016/S0074-7742(05)68006-3.
30. Brookes, M. J.; Vrba, J.; Robinson, S. E.; Stevenson, C. M.; Peters, A. M.; Barnes, G. R.; Hillebrand, A.; Morris, P. G. Optimising experimental design for MEG beamformer imaging. *Neuroimage* **2008**, *39*, 1788–802, doi:10.1016/j.neuroimage.2007.09.050.